

Anomalous CMB north-south asymmetry

Armando Bernui^{1,*}

¹*Instituto Nacional de Pesquisas Espaciais
Divisão de Astrofísica*

Av. dos Astronautas 1758, 12227-010 – São José dos Campos, SP, Brazil

(Dated: October 25, 2018)

Several accurate analyses have revealed a statistically significant North-South ecliptic asymmetry in the large-angle correlations strength of the Cosmic Microwave Background (CMB) radiation temperature field data from the Wilkinson Microwave Anisotropy Probe (WMAP). This asymmetry is inconsistent with the statistical isotropy expected in the concordance cosmological model Λ CDM. It has been suggested that a possible cause-effect relationship exists between this large-angle anisotropy and the anomalous CMB quadrupole-octopole planes alignment. In turn, this later phenomenon (or both) would be a consequence of one or more of the following undesired effects in CMB data: a systematic error in the data processing or in the instrument characterization, residual foregrounds, and large-angle correlations induced by the incomplete sky CMB data (cut-sky masks are needed to reject Galactic foregrounds). Here, it is proved that the North-South asymmetry is unrelated to the quadrupole ($\ell = 2$) and the octopole ($\ell = 3$) properties because we find, at high confidence levels, such large-angle anisotropy in three- and five-year WMAP CMB maps containing only the multipole components $4 \leq \ell \leq 10$. The statistical significance depends on both, the CMB map analyzed as well as the cut-sky mask applied to exclude foregrounds. In general, we obtain that the significance level of the North-South asymmetry is less in five-year WMAP data with KQ75 ($\gtrsim 90\%$ CL) than it is in three-year data with Kp0 ($\gtrsim 96\%$ CL). For instance, in the WMAP ILC-five-year map with the KQ75 mask (a sky cut of 28.4%) this phenomenon is observed at 92.7% CL, whereas for the WMAP ILC-three-year map with the Kp0 mask (a sky cut of 23.5%) this phenomenon appears at 96.5% CL. Moreover, it is also shown that this hemispherical asymmetry is unlikely due to systematics or foreground contaminants, because it is present in single-frequency, multifrequency, and cleaned ILC-type CMB maps. Additionally, robustness tests show that the statistical significance of the North-South asymmetry is affected by the use of the KQ85 and KQ75 masks in five-year single-frequency WMAP CMB maps, whereas it is insensitive with respect to application of the Kp2 and Kp0 masks in three-year single-frequency WMAP CMB maps. The confidence levels were obtained using sets of Monte Carlo CMB maps produced according to the Λ CDM model.

PACS numbers: 98.80.Es, 98.65.Dx, 98.70.Vc

I. INTRODUCTION

The five-year data release from the Wilkinson Microwave Anisotropy Probe (WMAP) [1, 2, 3, 4, 5] have recently confirmed the validity of the concordance cosmological model Λ CDM, which successfully describes the contents and evolution of the Universe. These, almost full-sky, precise cosmological data offer the unusual possibility to scrutinize the large-scale properties of the Universe, in particular those expected within this concordance model. One of these features concerns the set of Cosmic Microwave Background (CMB) radiation temperature fluctuations which is assumed to be a stochastic realization of a Gaussian random field, implying that their angular distribution on the celestial sphere is statistically isotropic at all angular scales. Examinations of the CMB maps from the first-year [6, 7, 8] and three-year WMAP data [9, 10, 11] have revealed highly significant departures from statistical isotropy, at large angular scales. Evidences of anomalous large-angle anisotropies

come from the power asymmetry of the CMB angular correlations between the northern and southern ecliptic hemispheres (hereafter NS-asymmetry), with indications of a preferred axis of maximum hemispherical asymmetry [12, 13, 14, 15, 16, 17, 18, 19, 20, 21, 22, 23, 24, 25, 26, 27, 28, 29, 30, 31, 32, 33, 34, 35] (for a different point of view see, e.g., [36, 37, 38, 39, 40, 41]). Furthermore, other manifestations of CMB large-angle anomalies include the unlikely quadrupole-octopole planes alignment (referring both to the strong planarity of these multipoles as well as to the alignment between such planes [21, 22, 23, 42, 43, 44, 45]). Other unexpected results include deviations from Gaussianity [46, 47, 48, 49, 50, 51, 52, 53].

Attempts to explain anomalous CMB phenomena have also considered globally axisymmetric space-times [55, 56, 57, 58, 59, 60], motivated by the fact that CMB data seem to indicate a preferred direction in the space. Other studies, instead, have investigated physical mechanisms that break statistical isotropy, or during the epoch of inflation [61, 62, 63, 64, 65, 66] or during the decoupling era [67, 68, 69, 70, 71, 72, 73], in order to account for two (or more) large-angle CMB anomalies. The motivation for searching a scenario that correlates two CMB anomalies is to comprehend whether these phenomena have

*bernui@das.inpe.br

different causes or instead they are manifestations of a unique effect. For this, a number of studies have searched for a possible relationship between the NS-asymmetry and the CMB quadrupole-octopole alignment phenomena (see, e.g., [21, 29, 73, 74]).

Although the origin of these CMB anomalies remains unknown, possible sources include CMB residual foregrounds [75, 76, 77, 78, 79, 80, 81], and systematic errors [19, 22, 82, 83]. In particular, there are indications that unremoved contaminants [84] or omitted systematics [85] could be influencing the reconstruction of the CMB quadrupole and octopole. Moreover, the WMAP cut-sky masks used to remove residual foregrounds probably induce spurious large-angle correlations, producing forged low-order CMB multipoles [86]. Thereby efforts are being done by the WMAP science team to improve the data processing by minimizing the effects caused by foregrounds and systematic errors [2, 10].

Here we show that the NS-asymmetry phenomenon is not related to the CMB's quadrupole or octopole components. To obtain this result we perform a two-point angular correlations analysis in an array of large-angle spherical caps that scan the CMB sky, where the WMAP maps investigated have their corresponding quadrupole and octopole components removed. The outline of this paper is the following. In Sec. II, we present the geometrical-statistical method, termed *sigma map*, that led us to investigate the directional angular correlations strength in a set of WMAP CMB maps. In Sec. III we first discuss the maps to be analyzed, after that we apply our method to these CMB data, where the statistical confidence is evaluated according to Monte Carlo maps produced according to the Λ CDM model. Finally, in Sec. IV, we formulate our conclusions and final remarks.

II. THE 2PACF AND THE SIGMA-MAP METHOD

Our method to investigate the large-scale angular correlations in CMB temperature fluctuations maps consists in the computation of the 2-point angular correlation function (2PACF) [88] in a set of spherical caps covering the celestial sphere.

Let $\Omega_{\gamma_0}^J \equiv \Omega(\theta_J, \phi_J; \gamma_0) \subset \mathcal{S}^2$ be a spherical cap region on the celestial sphere, of γ_0 degrees of aperture, with vertex at the J -th pixel, $J = 1, \dots, N_{\text{caps}}$, where (θ_J, ϕ_J) are the angular coordinates of the J -th pixel's center. Both, the number of spherical caps N_{caps} and the coordinates of their centers (θ_J, ϕ_J) are defined using the HEALPix pixelization scheme [87]. The union of the N_{caps} spherical caps covers completely the celestial sphere \mathcal{S}^2 .

Given a pixelized CMB map, the 2PACF of the temperature fluctuations δT corresponding to the pixels located in the spherical cap $\Omega_{\gamma_0}^J$ is defined by [88]

$$C(\gamma)^J \equiv \langle \delta T(\theta_i, \phi_i) \delta T(\theta_{i'}, \phi_{i'}) \rangle, \quad (1)$$

where $\cos \gamma = \cos \theta_i \cos \theta_{i'} + \sin \theta_i \sin \theta_{i'} \cos(\phi_i - \phi_{i'})$, and $\gamma \in (0, 2\gamma_0]$ is the angular distance between the i -th and the i' -th pixels centers. The average $\langle \rangle$ in the above equation is done over all the products $\delta T(\theta_i, \phi_i) \delta T(\theta_{i'}, \phi_{i'})$ such that $\gamma_k \equiv \gamma \in ((k-1)\delta, k\delta]$, for $k = 1, \dots, N_{\text{bins}}$, where $\delta \equiv 2\gamma_0/N_{\text{bins}}$ is the bin-width. We denote by $C_k^J \equiv C(\gamma_k)^J$ the value of the 2PACF for the angular distances $\gamma_k \in ((k-1)\delta, k\delta]$. Define now the scalar function $\sigma : \Omega_{\gamma_0}^J \subset \mathcal{S}^2 \mapsto \mathfrak{R}^+$, for $J = 1, \dots, N_{\text{caps}}$, which assigns to the J -cap, centered at (θ_J, ϕ_J) , a real positive number $\sigma_J \equiv \sigma(\theta_J, \phi_J) \in \mathfrak{R}^+$. The most natural way of defining a measure σ is through the variance of the C_k^J function [31],

$$\sigma_J^2 \equiv \frac{1}{N_{\text{bins}}} \sum_{k=1}^{N_{\text{bins}}} (C_k^J)^2. \quad (2)$$

To obtain a quantitative measure of the angular correlations in a CMB map, we cover the celestial sphere with N_{caps} spherical caps, and calculate the set of sigma values $\{\sigma_J, J = 1, \dots, N_{\text{caps}}\}$ using Eq. (2). Associating the J -th sigma value σ_J to the J -th pixel, for $J = 1, \dots, N_{\text{caps}}$, one fills the celestial sphere with positive real numbers, and according to a linear scale (where $\sigma^{\text{minimum}} \rightarrow \text{blue}$, $\sigma^{\text{maximum}} \rightarrow \text{red}$), one converts this numbered map into a colored map: this is the sigma map. Finally, we find the multipole components of a sigma map by calculating its angular power spectrum. In fact, given a sigma map one can expand $\sigma = \sigma(\theta, \phi)$ in spherical harmonics: $\sigma(\theta, \phi) = \sum_{\ell, m} A_{\ell m} Y_{\ell m}(\theta, \phi)$. Then, the set of values $\{S_\ell, \ell = 1, 2, \dots\}$, where $S_\ell \equiv (1/(2\ell+1)) \sum_{m=-\ell}^{\ell} |A_{\ell m}|^2$, give the angular power spectrum of the sigma map.

A power spectrum S_ℓ^{WMAP} of a sigma map computed from a given WMAP map, provides quantitative information about large-angle anisotropy features of such a CMB map when compared with the mean of sigma-map power spectra obtained from Monte Carlo CMB maps produced under the statistical isotropy hypothesis. As we shall see, the sigma-map analysis is a suitable tool to reveal large-angle anisotropies in CMB maps, like the NS-asymmetry.

III. CMB ANALYSES WITH THE SIGMA MAP

In this section, we apply the sigma-map method to study the large-angle correlations in a set of single- and multifrequency CMB temperature fluctuations maps, all coming from the three-year and five-year WMAP data.

A. The WMAP data

The WMAP science team made substantial efforts to improve the data products by minimizing the contaminating effects caused by diffuse Galactic foregrounds, astrophysical point sources, artifacts from the instruments

and measurement process, and systematic errors [2, 10]. As a result, it has been released as the single-frequency CMB foreground-reduced Q-, V-, and W-band maps corresponding to the less contaminated frequencies centered at 41, 61, and 94 GHz, respectively (hereafter the Q-5yr, V-5yr, and W-5yr maps, respectively), and an Internal Linear Combination (ILC-5yr) full-sky CMB map [9]. Moreover, the eight foreground-reduced differencing assemblies (two in the Q-band, two in the V-band, and four in the W-band) can be combined using inverse-noise-variance weights to produce multifrequency CMB maps, like the QVW and the VW coadded maps, hereafter termed QVW-5yr and VW-5yr maps [8]. The corresponding three-year maps are the Q-3yr, V-3yr, W-3yr, ILC-3yr, QVW-3yr, and VW-3yr CMB maps [9]. In addition to these maps, other teams have also produced full-sky cleaned CMB maps using the unprocessed three-year and five-year data through different foreground cleaning tools, that is, the de Oliveira-Costa-Tegmark [77], the Park-Park-Gott [23], and the Kim-Naselsky-Christensen CMB maps [89], hereafter termed the OT-3yr, PPG-3yr, and KNC-5yr, respectively.

In order to validate our sigma-map results we shall estimate their sensitivity to the following effects, which are possible sources of large-angle anomalies in WMAP data: (i) residual foregrounds, (ii) masking applications, (iii) systematic errors (coming from, e.g., instrument noise, foreground-minimization process, time-ordered data analysis, etc.). Regarding the issue (i), we know that the Galactic foregrounds are frequency dependent [7]. For this reason the study of the individual frequency CMB maps, that is the foreground-reduced Q, V, and W three- and five-year maps are essential to detect the possible contribution of Galactic contaminants in our results. Moreover, following the WMAP science team recommendation to reject foregrounds contamination in temperature analyses in five-year (three-year) data we use the Galactic mask KQ85 (Kp2), which cuts 18.3% (15.4%) of the sky data [2, 4]. Regarding issue (ii), we shall test the sensitivity of our results due to the masking application by comparing the effects due to the more severe five-year KQ75 (three-year Kp0) mask, which cuts 28.4% (23.5%) of the sky data, with respect to the KQ85 (Kp2) mask. Regarding issue (iii), we know that (large-angle) systematic effects leave (large-angle) imprints in the CMB maps [1, 2, 3, 10]. Because we are investigating a large-scale anisotropy, that is the NS-asymmetry phenomenon, we intend to avoid possible large-angle systematic effects. According to recent reports the quadrupole and the octopole CMB components could be contaminated with systematics, e.g., in the time-ordered data analyses [19, 22, 85], or due to the masking procedures [86]. Furthermore, systematics could also appear in the foreground-decontamination processes [80, 81, 82, 83, 84]. For these reasons, we study the large-scale properties of the CMB temperature field in WMAP data containing just the multipoles $4 \leq \ell \leq 10$, that is, removing the quadrupole ($\ell = 2$) and

the octopole ($\ell = 3$) CMB components. Moreover, we investigate all the publicly available cleaned maps just to exclude the possibility that a particular foreground-minimization process is introducing systematic effects in the data.

Our aim is to investigate the large-scale angular distribution of the CMB temperature fluctuations. Given a CMB map, we shall concentrate on the submap containing the set of multipole components $4 \leq \ell \leq 10$. To produce this submap, containing the CMB temperature fluctuations information at these angular scales, we first use the ANAFast code [87] to obtain, after applying a cut-sky mask, the $\{a_{\ell m}\}$ values corresponding to these multipoles. Then, using the SYNFAST code [87], we use this set $\{a_{\ell m}\}$ to make up the CMB map. We emphasize that, all the CMB maps here investigated using the sigma-map analysis only contain the multipole components $4 \leq \ell \leq 10$, and we adopt the following notation: for instance, the ILC-5yr-KQ85 map is obtained from the ILC-5yr CMB map by selecting, after applying the KQ85 mask, those multipoles in the range $4 \leq \ell \leq 10$.

We generate one set of 1 000 Monte Carlo CMB maps (MC) which correspond to random realizations seeded by the Λ CDM angular power spectra [4], with $N_{\text{side}} = 512$, and $\ell_{\text{max}} = 1024$. From this MC set we produced two sets of 1 000 MC each for the multipole range $4 \leq \ell \leq 10$ after using the KQ85 and KQ75 masks, respectively. The statistical significance analyses come from the comparison between the angular power spectra of the sigma maps obtained from the WMAP data (hereafter sigma-maps WMAP) and the corresponding angular power spectra calculated from the sigma maps computed from the MC CMB maps (hereafter sigma-maps MC).

B. Data analyses with the KQ85 and KQ75 masks

Our objective here is to produce the sigma-maps WMAP for each of the five-year (three-year) WMAP maps mentioned above, containing the multipoles $4 \leq \ell \leq 10$ obtained after using the KQ85 (Kp2) cut-sky mask. After the calculation of the sigma-maps WMAP we compute their corresponding angular power spectra $\{S_{\ell}, \ell = 1, \dots, 5\}$ in order to quantify, by comparison with the corresponding set of sigma-maps MC, if they are consistent, or not, with statistically isotropic Λ CDM CMB maps.

To illustrate our results we show in Fig. 1 (Fig. 2), from top to bottom, the ILC-5yr-KQ85 (ILC-5yr-KQ75) CMB map, and its corresponding sigma-maps WMAP, computed for three different γ_0 values, that is, $\gamma_0 = 30^\circ, 45^\circ, 60^\circ$. As we observe, these sigma-maps WMAP clearly exhibit a dipolar red-blue region strongly indicative of a large-angle asymmetry in the distribution of the angular correlations, the so-called NS-asymmetry phenomenon (in all sky maps we have used Galactic coordinates where the equator is defined by the latitude $b = 90^\circ$, with the Galactic center $(l, b) = (0, 90^\circ)$ in the

middle of the figure, and the longitude l increases to the left).

To quantify this NS-asymmetry in the sigma-maps-WMAP-KQ85 and sigma-maps-WMAP-5yr-KQ75, we calculate their angular power spectra, and then evaluate their statistical significance by comparison with the corresponding sigma-maps MC's angular power spectra. Our results appear in the top-panel plots of Figs. 3 and 4 corresponding to the WMAP-KQ85 and WMAP-5yr-KQ75 cases, respectively, where solid lines represent the mean values obtained from sigma-maps MC and dashed lines represent the 95% CL from these data. In each case the MC data contain the multipoles $4 \leq \ell \leq 10$ obtained after applying the corresponding KQ85 or KQ75 cut-sky mask. Notice that in Figs. 3 and 4 the symbols representing data from three-year sigma-maps WMAP are plotted (in red) close to the vertical axis, while the symbols representing data from the five-year sigma-maps WMAP are plotted (in blue) slightly shifted to the right. This is done in order to observe the differences outcoming from distinct data releases. For illustration, in the bottom panels of Figs. 3 and 4 we plotted the dipole components of the sigma-map-ILC-5yr KQ85 and sigma-map-ILC-5yr KQ75, respectively, where we observe that both dipoles point nearly in the same direction $(l, b) \simeq (180^\circ, 130^\circ)$, which means that this result is stable with respect to the choice of the KQ85 and KQ75 Galactic masks.

The sigma-maps WMAP angular power spectra shown at the top panels of Figs. 3 and 4, were obtained using spherical caps of aperture $\gamma_0 = 45^\circ$, $N_{\text{bins}} = 45$, and $N_{\text{caps}} = 768$. For calculating the sigma maps we used CMB maps with pixelization parameter $N_{\text{side}} = 32$. Concerning the robustness of our results, we studied the effects of changing various parameters employed in the calculation of the sigma maps. Our tests included the computation of the sigma maps using spherical caps of $\gamma_0 = 30^\circ, 45^\circ, 60^\circ$ of aperture, also considering different $N_{\text{bins}} = 45, 90, 120$ values, and $N_{\text{caps}} = 768, 3072$. Additionally, we also studied the influence of the angular resolution of the CMB maps by computing the sigma-maps WMAP with different pixelizations parameter, namely $N_{\text{side}} = 16, 32$. We found that the sigma-maps WMAP as well as their corresponding angular power spectra calculated in these cases are completely similar to those results exhibit in Figs. 3 and 4.

Examining data from the sigma-maps-WMAP KQ85, shown in the top panel of Fig. 3, we observe that the Q-3yr (bullet), V-3yr (asterisk), and W-3yr (star) data do not show significative differences between them, but the Q-5yr (bullet), V-5yr (asterisk), and W-5yr (star) data exhibit very different dipole values. In fact, the confidence level values for the dipole values $S_1^{\text{Q-3yr}}$, $S_1^{\text{V-3yr}}$, $S_1^{\text{W-3yr}}$ are 95.1%, 95.7%, and 95.9% CL, respectively, whereas for $S_1^{\text{Q-5yr}}$, $S_1^{\text{V-5yr}}$, $S_1^{\text{W-5yr}}$ are 85.9%, 95.8%, and 99.5% CL, respectively. These differences in WMAP-KQ85 five-year data suggest the presence of residual foregrounds in Q-5yr, V-5yr, and W-5yr maps. On the other

hand, the Q-3yr, V-3yr, and W-3yr maps appear to be foreground cleaned enough. Nevertheless, the quantitative analysis shown at the top panel of Fig. 3 confirms the NS-asymmetry phenomenon, at 95% – 99% CL, for all (except one of) the WMAP-KQ85 CMB maps analyzed. The exception is due to the Q-5yr-KQ85 map. We emphasize that these results are independent of the CMB quadrupole ($\ell = 2$) and octopole ($\ell = 3$) components because they were completely removed before we began our analyses.

Regarding the quantitative sigma-map analysis for the WMAP-KQ75 CMB maps, top panel of Fig. 4, we verify that the NS-asymmetry phenomenon is present, at more than 98% CL, in all the single, multifrequency, and ILC-type WMAP-3yr-Kp0 maps and also in the KNC-5yr-KQ75 foreground cleaned map. In all the other WMAP-5yr-KQ75 maps the NS-asymmetry phenomenon appears with a lower statistical significance. It is worth noting, again, that the dipole values S_1 from single frequency Q-, V-, W-5yr-KQ75 maps are disperse, on the contrary, again, the dipole values S_1 from single frequency Q-, V-, W-3yr-Kp0 maps are clustered, a distinct behavior that suggests the presence of residual foregrounds, deserving further analysis.

The possibility that foregrounds were not completely removed with the application of the KQ85 mask motivate further analysis of the WMAP data through the use of the more severe cut-sky KQ75 mask. Analyzing our results from the sigma-maps-WMAP-5yr KQ75 and sigma-maps-WMAP-3yr Kp0, shown in the top panel of Fig. 4, we observe that the confidence level for the dipole values $S_1^{\text{Q-3yr}}$, $S_1^{\text{V-3yr}}$, $S_1^{\text{W-3yr}}$ are 95.6%, 96.3%, and 96.7% CL, respectively, whereas for $S_1^{\text{Q-5yr}}$, $S_1^{\text{V-5yr}}$, $S_1^{\text{W-5yr}}$ are 89.2%, 90.9%, and 93.7% CL, respectively. We observe that the application of the more severe KQ75 cut-sky mask produces a lower dispersion of the confidence levels for these dipoles (mean = $91.3 \pm 2.3\%$ CL) as compared with the KQ85 mask case (mean = $93.7 \pm 7.0\%$ CL), but it is still large as compared with the WMAP-3yr case. In fact, the dipole terms corresponding to the single-frequency Q-3yr, V-3yr, and W-3yr WMAP maps have their mean and standard deviation: $96.2 \pm 0.6\%$ CL and $95.6 \pm 0.4\%$ CL for the Kp0 and Kp2 masks, respectively. This later result reveals two important consequences regarding the single-frequency WMAP-3yr maps: first, these CMB maps appear sufficiently foreground cleaned, and second, the NS-asymmetry phenomenon exhibited in three-year WMAP data is robust with respect to the Kp0 and Kp2 masks. From other side, the masking-dependent and disperse results achieved in the analysis of the single-frequency Q-5yr, V-5yr, and W-5yr maps could indicate possible unremoved foregrounds, regardless of the severe KQ75 mask applied.

Additionally, a close inspection of the data plotted in the top panel of Fig. 4 reveals another interesting feature concerning the WMAP-ILC maps and the applied masks. We notice that the statistical significance for the dipole value of the sigma-map-ILC-5yr KQ75 is 92.7%

CL, whereas for the dipole value of the sigma-map-ILC-5yr Kp0 is 96.5% CL, which shows a $\sim 4\%$ difference. From other side, one verifies that the ILC-5yr-KQ75 and ILC-3yr-Kp0 CMB maps are fully similar as revealed by the Pearson's correlation coefficient: 0.985180 and 0.985466, for the CMB data outside the KQ75 and Kp0 masks, respectively, which are only $\sim 0.03\%$ different. The question is, why highly correlated CMB maps give such dissimilar (sigma-map) results? The answer involves a twofold aspect of a given mask: the amount of the sky cutted by the mask and the location of the sky-patch cutted. These important issues, related to the robustness of our results, motivate a masking-effect analysis on the angular power spectra of the sigma-maps WMAP.

C. Masking-effect analysis: KQ75 versus Kp0

Observing the data plotted in the top panel of Fig. 4, one realizes that the spectra from sigma-map-3yr-Kp0 data have consistently larger values than the spectra from sigma-map-5yr KQ75. This fact could be indicating a systematic effect due to the different masks, KQ75 and Kp0, employed in these calculations. Clearly, the use of these two masks involves two effects: the different amount of cutted sky, of $\sim 5\%$ between the KQ75 and Kp0 masks, and the sky location of the cutted patch. A consequence of the first effect is that different sky regions with CMB data are being considered to make up the WMAP-KQ75 and WMAP-Kp0 maps, which implies distinct contributions into their corresponding sigma maps; a consequence of the second effect is that depending on the location of the cutted region, the calculation of the 2PACF for the sigma map could be strengthened or weakened. In both cases, we are introducing (positive or negative) spurious correlations in the sigma maps whose influence on our results need to be examined. The study of the masking effects on the sigma maps is connected with the second issue mentioned in III A.

For this, we perform a comparative sigma-map analysis of the four CMB maps: ILC-3yr-KQ75, ILC-3yr-Kp0, ILC-5yr-KQ75, and ILC-5yr-Kp0. In other words, we shall test the sensitivity of the ILC-3yr and ILC-5yr CMB maps to the effect of interchanging the use of KQ75 and Kp0 masks to obtain the multipoles components $4 \leq \ell \leq 10$. Our results are shown in Fig. 5. In the top panel we plot the sigma-map spectra of these four CMB maps, that is, $\{S_\ell^{\text{ILC-3yr-KQ75}}\}$, $\{S_\ell^{\text{ILC-3yr-Kp0}}\}$, $\{S_\ell^{\text{ILC-5yr-KQ75}}\}$, and $\{S_\ell^{\text{ILC-5yr-Kp0}}\}$, represented as circle, filled-circle, square, and filled-square symbols, respectively. Our results show

$$\begin{aligned} S_\ell^{\text{ILC-3yr-KQ75}} &\simeq S_\ell^{\text{ILC-5yr-KQ75}} \\ S_\ell^{\text{ILC-5yr-Kp0}} &\simeq S_\ell^{\text{ILC-3yr-Kp0}} \end{aligned} ,$$

proving that the main reason (if not the unique one) for the different spectra values corresponding to the three- and five-year sigma-maps ILC is the distinct cut-sky area

defined by the KQ75 and Kp0 masks. Additionally, we find it interesting to know the contrasting effect produced by these two masks in the sigma-map-ILC-5yr KQ75 and sigma-map-ILC-5yr Kp0. For this we present at the bottom panel of Fig. 5 the difference map: sigma-map-ILC-5yr Kp0 minus sigma-map-ILC-5yr KQ75, which clearly reveals through its red-intense spots that the application of different masks has a significant impact on the detection of the NS-asymmetry phenomenon (the corresponding difference map for ILC-3yr case is fully similar). Observing this difference map we understand why the use of the KQ75 mask decreases the statistical significance of the NS-asymmetry phenomenon: this mask cuts a sky-patch that turns out to be critical for the computation of the large-scale 2PACF in the sigma-maps.

To illustrate the full-sky case, that is a sigma-map analysis of the foreground-cleaned ILC-5yr CMB map with multipoles $4 \leq \ell \leq 10$ obtained without using a mask, we show in Fig. 6 the sigma-map-ILC-5yr (top panel) and its corresponding dipole term (bottom panel). The statistical significance of this sigma-map-ILC 5yr, as compared with 1000 sigma-maps MC obtained from an equal number of full-sky ΛCDM MC- ℓ_{4-10} CMB maps, is 95.8% CL.

IV. CONCLUSIONS

We investigated a set of foregrounds-reduced and systematics-cleaned single-frequency, multifrequency, and ILC-type CMB maps from three- and five-year WMAP data. We performed the sigma-maps analyses of these CMB maps at large-angles corresponding to the multipoles range $4 \leq \ell \leq 10$, and for different three- and five-year WMAP cut-sky masks, that is Kp2, Kp0, KQ85, and KQ75.

We found that the single-frequency Q-3yr, V-3yr and W-3yr WMAP maps show, independently of the mask (Kp2 or Kp0) used to obtain the multipoles $4 \leq \ell \leq 10$, the same sigma-map angular power spectra with confidence level $\sim 96\%$ in all the cases (see in the top panel of Fig. 3, symbols plotted close to the vertical line). This result indicates, at least concerning the sigma-map analysis, that the single-frequency Q-3yr, V-3yr, and W-3yr maps are reasonable foreground cleaned. As a consequence, the multifrequency CMB maps, that is VW, QVW, and ILC-type, produced with these single-frequency maps behaves accordingly. For the WMAP-5yr-KQ85 data (see in the top panel of Fig. 3, symbols plotted slightly shifted to the right) we found in all, but one, of these CMB maps, at 95% – 99% CL, an uneven hemispherical distribution in the intensity of the two-point large-angle temperature correlations. The exceptional case refers to the Q-5yr map. On the contrary the single-frequency Q-5yr, V-5yr and W-5yr WMAP maps exhibit a disparate behavior as seen in their corresponding sigma-map angular power spectra, in both KQ85 and KQ75 mask cases. This probably suggests that these

CMB maps have residual foregrounds that diminish but are not fully eliminated with the use of the more severe KQ75 mask.

We also notice, despite that the ILC-5yr-KQ75 and the ILC-3yr-Kp0 CMB maps are fully correlated (Pearson's correlation coefficient: 0.985180 and 0.985466, for the CMB data outside the KQ75 and Kp0 masks) their corresponding sigma maps are not so much. This fact motivated a detailed examination of the masking effects on the sigma-map angular power spectra. To estimate the influence of the different masks employed we calculate the sigma maps for the ILC-3yr CMB map obtained after applying the five-year KQ75 mask, and for the ILC-5yr CMB map after applying the three-year Kp0 mask. The angular power spectra of sigma-map-3yr-KQ75, sigma-map-3yr-Kp0, sigma-map-5yr-KQ75, and sigma-map-5yr-Kp0 data are shown in the top panel of Fig. 5. We conclude that the KQ75 mask, as compared with Kp0, has a significant impact on the detection of the NS-asymmetry phenomenon decreasing its statistical significance. In fact, the KQ75 mask cuts a sky patch that turns out to be critical for the computation of the large-scale 2PACF in the sigma maps (as revealed by the difference map: sigma-map-ILC-5yr Kp0 minus sigma-map-ILC-5yr KQ75, plotted at the bottom panel of Fig. 5).

Summarizing, first, our results prove that the NS-asymmetry phenomenon is present at the large angular scales defined by the CMB multipoles $4 \leq \ell \leq 10$, at a high significance level, in a set of single and multi-frequency CMB maps from three- and five-year WMAP data, where the statistical significance depends on both, the CMB map analyzed as well as the cut-sky mask applied to exclude foregrounds. In general, we obtain that the NS-asymmetry is statistically less significant in five-year WMAP data with KQ75 ($\gtrsim 90\%$ CL) than it is in three-year data with Kp0 ($\gtrsim 96\%$ CL). For instance, in the ILC-5yr-KQ75 map the NS-asymmetry is observed at 92.7% CL, whereas in the ILC-3yr-Kp0 map this phenomenon appears at 96.5% CL. Second, these results also show that the NS-asymmetry in WMAP maps is unrelated to the quadrupole and octopole CMB compo-

nents because they were removed from the CMB maps in our analysis. Third, due to the whole set of sensitivity tests performed our results strongly suggest that this hemispherical power asymmetry, is unlikely correlated with spurious phenomena like residual foregrounds, masking applications, or known systematic effects. Additionally, we found that the statistical significance of the NS-asymmetry phenomenon is affected by the use of the KQ85 and KQ75 masks in five-year single-frequency WMAP CMB maps, whereas it is insensitive with respect to application of the Kp2 and Kp0 masks in three-year single-frequency WMAP CMB maps. Moreover, we also examined satisfactorily the robustness of our results under several parameters used in the application of the sigma-map method. The statistical significance of the sigma-maps-WMAP angular power spectra were calculated by comparing them against those obtained from 1 000 Monte Carlo CMB maps produced in agreement with the WMAP Λ CDM concordance model [4]. Finally, as an illustrative case, we also performed the sigma-map analysis for the full-sky ILC-5yr- ℓ_{4-10} CMB map, where we find the NS-asymmetry phenomenon at 95.8% CL for the angular scales $4 \leq \ell \leq 10$, a result that is independent of the quadrupole and octopole CMB components. For completeness, we plot in Fig. 6 the sigma-map-ILC-5yr- ℓ_{4-10} (top panel) and its corresponding dipole term (bottom panel), which reveals that the NS-asymmetry axis for the ILC-5yr- ℓ_{4-10} map points along the direction $(l, b) \simeq (220^\circ, 120^\circ)$.

Acknowledgements

I am grateful for the use of the Legacy Archive for Microwave Background Data Analysis (LAMBDA). Some of the results in this paper have been derived using the HEALPix package [87]. I acknowledge I.S. Ferreira, C.A. Wuensche, A.F.F. Teixeira, and T. Villela for insightful comments and suggestions. A.B. is supported by MCT PCI/DTI.

-
- [1] G. Hinshaw *et al.*, arXiv:0803.0732.
 - [2] B. Gold *et al.*, arXiv:0803.0715.
 - [3] J. Dunkley *et al.*, arXiv:0803.0586.
 - [4] M.R. Nolta *et al.*, arXiv:0803.0593.
 - [5] E. Komatsu *et al.*, arXiv:0803.0547.
 - [6] C.L. Bennett *et al.*, *Astrophys. J. Suppl. Ser.* **148**, 1 (2003).
 - [7] C.L. Bennett *et al.*, *Astrophys. J. Suppl. Ser.* **148**, 97 (2003).
 - [8] G. Hinshaw *et al.*, *Astrophys. J. Suppl. Ser.* **148**, 135 (2003).
 - [9] G. Hinshaw *et al.*, *Astrophys. J. Suppl. Ser.* **170**, 288 (2007).
 - [10] N. Jarosik *et al.*, *Astrophys. J. Suppl. Ser.* **170**, 263 (2007).
 - [11] D.N. Spergel *et al.*, *Astrophys. J. Suppl. Ser.* **170**, 377 (2007).
 - [12] F.K. Hansen, A.J. Banday, and K.M. Górski, *Mon. Not. R. Astron. Soc.* **354**, 641 (2004).
 - [13] F.K. Hansen, P. Cabella, D. Marinucci, and N. Vittorio, *Astrophys. J.* **607**, L67 (2004).
 - [14] P. Bielewicz, K.M. Górski, and A.J. Banday, *Mon. Not. R. Astron. Soc.* **355**, 1283 (2004).
 - [15] H.K. Eriksen, F.K. Hansen, A.J. Banday, K.M. Górski, and P. B. Lilje, *Astrophys. J.* **605**, 14 (2004).
 - [16] H.K. Eriksen, A.J. Banday, K.M. Górski, and P.B. Lilje, *Astrophys. J.* **622**, 58 (2005).
 - [17] K. Land and J. Magueijo, *Mon. Not. R. Astron. Soc.* **357**, (2007).

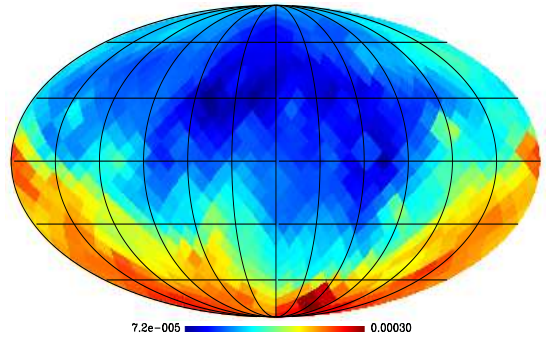
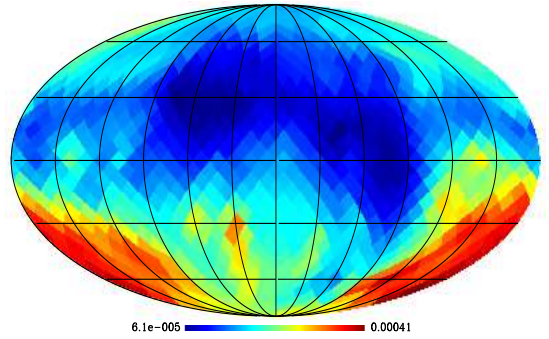
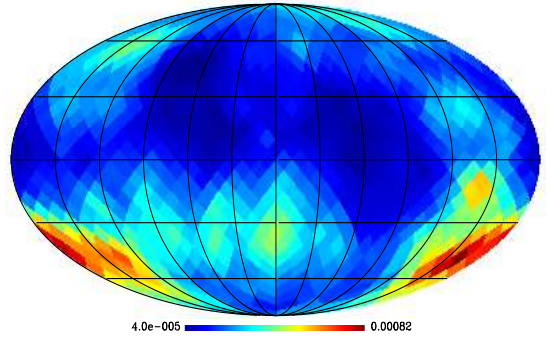
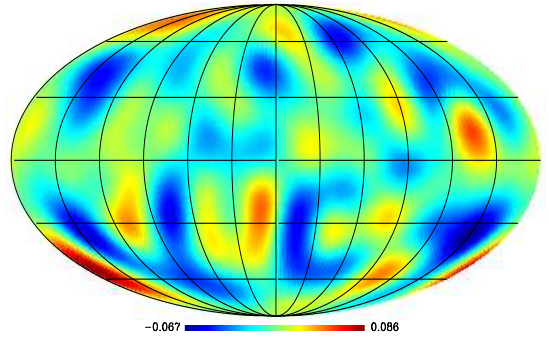
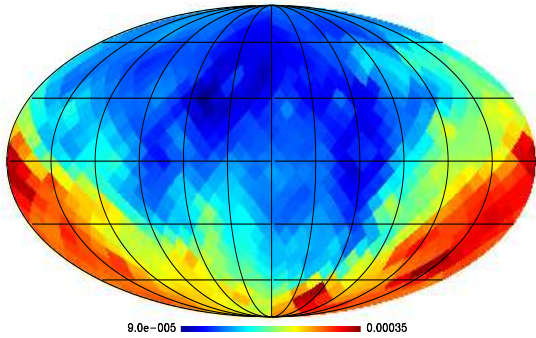
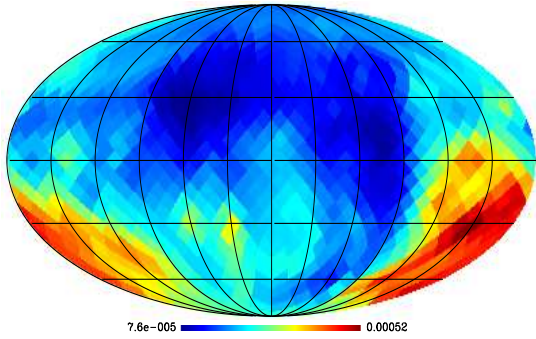
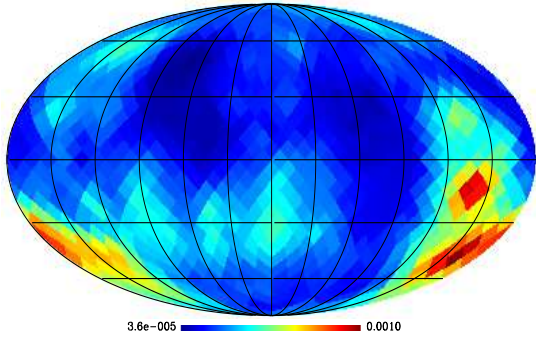
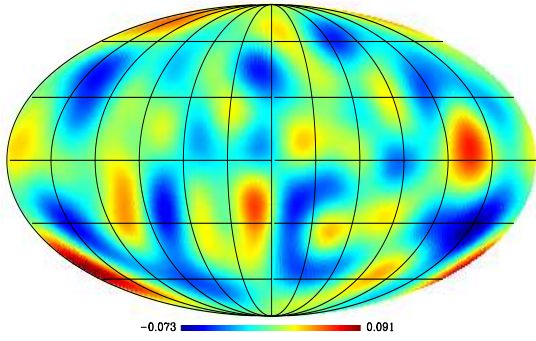


FIG. 1: The top panel shows the CMB map ILC-5yr-KQ85- ℓ_{4-10} . The second, third, and fourth panels are the sigma-maps calculated from this CMB map considering spherical caps with apertures $\gamma_0 = 30^\circ, 45^\circ, 60^\circ$, respectively. The NS-asymmetry is clearly seen in the uneven hemispherical distribution of the angular correlations strength, depicted as red and blue pixels (large and small sigma-values, respectively). All the maps are plotted in Galactic coordinates.

FIG. 2: The top panel shows the CMB map ILC-5yr-KQ75- ℓ_{4-10} . The second, third, and fourth panels are the sigma-maps calculated from this CMB map considering spherical caps with apertures $\gamma_0 = 30^\circ, 45^\circ, 60^\circ$, respectively. Again, the NS-asymmetry is clearly seen in the uneven hemispherical distribution of the angular correlations strength, depicted as red and blue pixels (large and small sigma-values, respectively). All the maps are plotted in Galactic coordinates.

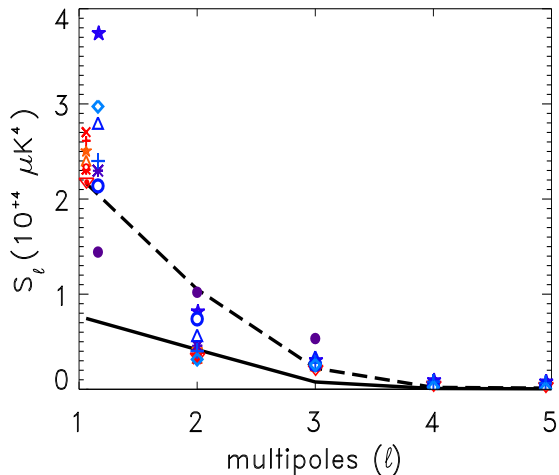


FIG. 3: Top: Angular power spectra S_ℓ of the sigma-maps-WMAP-KQ85- ℓ_{4-10} compared with the mean (solid line) and their corresponding 95% CL (dashed line) of 1000 sigma-maps MC, obtained from an equal number of MC-KQ85- ℓ_{4-10} CMB maps. The symbols representing data from three-year WMAP maps are plotted (in red) close to the vertical axis, while the symbols representing data from the five-year WMAP maps are plotted (in blue) slightly shifted to the right. The Q, V, W, VW, QVW, OT, PPG, KNC, and ILC CMB maps are represented by the bullet, asterisk, star, triangle, circle, nabla, \times , diamond, and $+$ symbols, respectively. The NS-asymmetry phenomenon in WMAP CMB maps is evidenced, except for the Q-5yr map, through the anomalously large dipole value of the sigma-maps-WMAP KQ85, at more than 95% CL. Bottom: This is the dipole term of the sigma-maps-ILC-5yr KQ85 obtained with $\gamma_0 = 45^\circ$ (actually the $\gamma_0 = 30^\circ, 60^\circ$ cases are similar), where we observe that it points in the direction $(l, b) \simeq (190^\circ, 130^\circ)$.

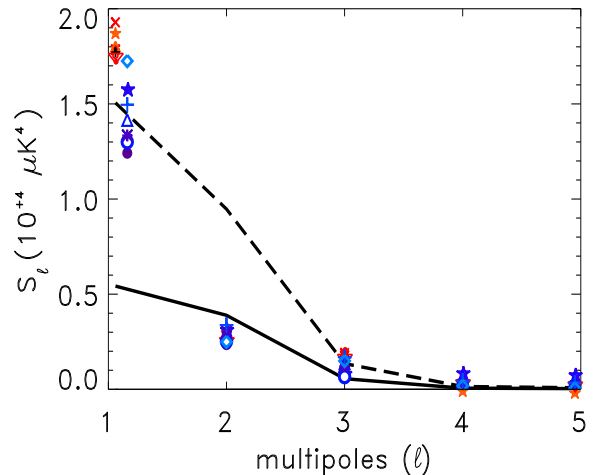


FIG. 4: Top: Angular power spectra S_ℓ of the sigma-maps-WMAP-KQ75- ℓ_{4-10} compared with the mean (solid line) and their corresponding 95% CL (dashed line) of 1000 sigma-maps MC, obtained from an equal number of MC-KQ75- ℓ_{4-10} CMB maps. The symbols representing data from three-year WMAP maps are plotted (in red) close to the vertical axis, while the symbols representing data from the five-year WMAP maps are plotted (in blue) slightly shifted to the right. The Q, V, W, VW, QVW, OT, PPG, KNC, and ILC CMB maps are represented by the bullet, asterisk, star, triangle, circle, nabla, \times , diamond, and $+$ symbols, respectively. We observe that the NS-asymmetry phenomenon in WMAP CMB maps is revealed at more than 98% CL, in all the single, multi-frequency, and ILC-type WMAP-3yr-Kp0 maps and also in the KNC-5yr-KQ75 foreground-cleaned map. However, in all the other sigma-maps-WMAP-5yr-KQ75 maps the statistical significance is lower, and this matter has been suitably analyzed in Sec. III C. Bottom: This is the dipole term of the sigma-maps-ILC-5yr KQ75 obtained with $\gamma_0 = 45^\circ$ (actually the $\gamma_0 = 30^\circ, 60^\circ$ cases are similar), where we observe that it points in the direction $(l, b) \simeq (180^\circ, 130^\circ)$.

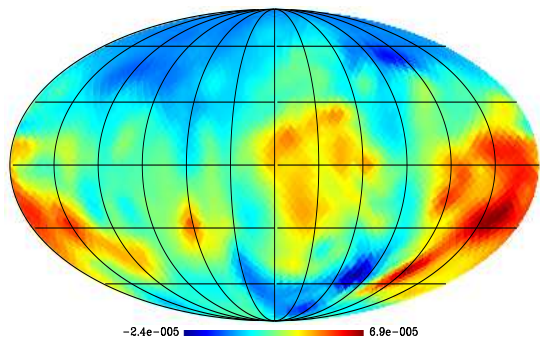
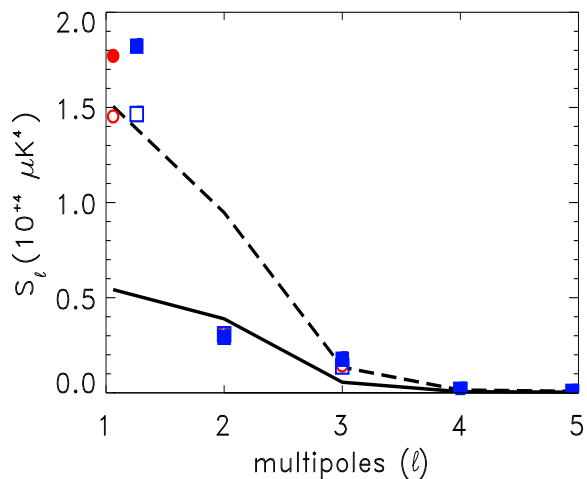


FIG. 5: Top: Sigma-map angular power spectra of the analyze CMB maps: ILC-3yr-KQ75, ILC-3yr-Kp0, ILC-5yr-KQ75, and ILC-5yr-Kp0, represented as circle, filled-circle (or bullet), square, and filled-square symbols, respectively. These results show that $S_{\ell}^{\text{ILC-3yr-KQ75}} \simeq S_{\ell}^{\text{ILC-5yr-KQ75}}$ and $S_{\ell}^{\text{ILC-5yr-Kp0}} \simeq S_{\ell}^{\text{ILC-3yr-Kp0}}$, demonstrating that the main reason for the different statistical significance found in Fig. 4 for the sigma-map-ILC-3yr and sigma-map-ILC-5yr is due to the distinct cut-sky area defined by the KQ75 and Kp0 masks. In fact, the NS-asymmetry phenomenon is present, at more than 96% CL, in those maps where the Kp0 mask has been applied (i.e., the ILC-3yr-Kp0 and ILC-5yr-Kp0 CMB maps). Bottom: This is the difference map: sigma-map-ILC-5yr-Kp0 minus sigma-map-ILC-5yr-KQ75, which clearly reveals through its red-intense spots that the application of different masks has a significant impact on the detection of the NS-asymmetry phenomenon: the KQ75 mask cuts a sky patch that turns out to be critical for the computation of the large-scale 2PACF in the sigma-maps.

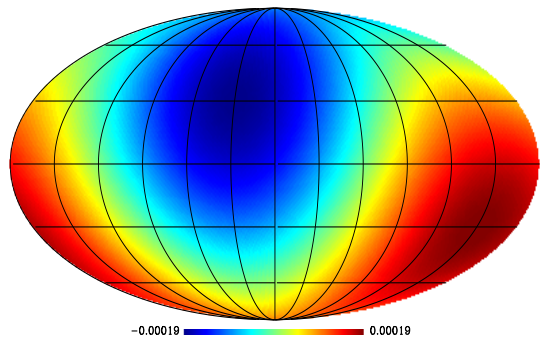
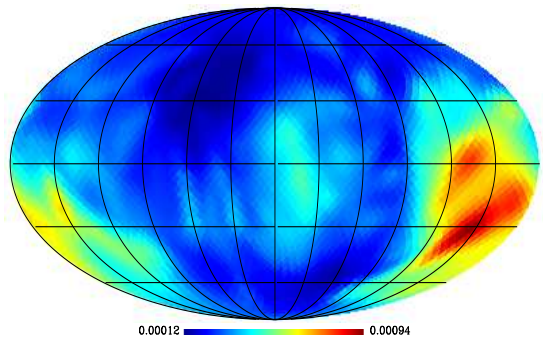


FIG. 6: For illustration we show the sigma-map-ILC-5yr- ℓ_{4-10} computed from the WMAP-ILC-5yr full-sky CMB map (top panel) and its corresponding dipole term (bottom panel). Observe that this dipole term is pointing in the direction $(l, b) \simeq (220^\circ, 120^\circ)$.

- 994 (2005).
- [18] K. Land and J. Magueijo, Phys. Rev. Lett. **95**, 071301 (2005).
- [19] C.J. Copi, D. Huterer, D.J. Schwarz, and G.D. Starkman, Mon. Not. R. Astron. Soc. **367**, 79 (2006).
- [20] A. Bernui, T. Villela, C.A. Wuensche, R. Leonardi, and I. Ferreira, Astron. & Astrophys. **454**, 409 (2006).
- [21] Y. Wiaux, P. Vielva, E. Martínez-González, and P. Vanderghenst, Phys. Rev. Lett. **96**, 151303 (2006).
- [22] C.J. Copi, D. Huterer, D.J. Schwarz, and G.D. Starkman, Phys. Rev. D **75**, 023507 (2007).
- [23] C.-G. Park, C. Park, and J.R. Gott III, Astrophys. J. **660**, 959 (2007).
- [24] D. Huterer, New Astronomy Reviews **50**, 868 (2006).
- [25] F.K. Hansen, A.J. Banday, H.K. Eriksen, K.M. Górski, and P. B. Lilje, Astrophys. J. **648**, 784 (2006).
- [26] P. Vielva, Y. Wiaux, E. Martínez-González, and P. Van-

- dergheynst, *New Astron. Rev.* **50**, 880 (2006).
- [27] P. Vielva, Y. Wiaux, E. Martínez-González, and P. Vandergheynst, *Mon. Not. R. Astron. Soc.* **381**, 932 (2007).
- [28] H.K. Eriksen, A.J. Banday, K.M. Górski, F.K. Hansen, and P.B. Lilje, *Astrophys. J.* **660**, L81 (2007).
- [29] K. Land and J. Magueijo, *Mon. Not. R. Astron. Soc.* **378**, 153 (2007).
- [30] P.K. Samal, R. Saha, P. Jain, and J.P. Ralston, *Mon. Not. R. Astron. Soc.* **385**, 1718 (2008).
- [31] A. Bernui, B. Mota, M.J. Rebouças, and R. Tavakol, *Astron. & Astrophys.* **464**, 479 (2007).
- [32] A. Bernui, B. Mota, M.J. Rebouças, and R. Tavakol, *Int. Journal of Mod. Phys. D* **16**, 411 (2007).
- [33] E.F. Bunn and A. Bourdon, arXiv:0808.0341.
- [34] C. Monteserín, R.B. Barreiro, P. Vielva, E. Martínez-González, M.P. Hobson, and A.N. Lasenby, *Mon. Not. R. Astron. Soc.* **387**, 209 (2008).
- [35] B. Lew, arXiv:0808.2867.
- [36] A. Hajian and T. Souradeep, *Astrophys. J.* **597**, L5 (2003).
- [37] A. Hajian, T. Souradeep, and N. Cornish, *Astrophys. J.* **618**, L63 (2005).
- [38] T. Souradeep and A. Hajian, *Pramana* **62**, 793 (2004).
- [39] T. Souradeep and A. Hajian, arXiv:0502248.
- [40] T. Souradeep, A. Hajian, and S. Basak, *New Astronomy Reviews* **50**, 889 (2006).
- [41] A. Hajian and T. Souradeep, *Phys. Rev. D* **74**, 123521 (2006).
- [42] M. Tegmark, A. de Oliveira-Costa, and A.J.S. Hamilton, *Phys. Rev. D* **68**, 123523 (2003).
- [43] A. de Oliveira-Costa, M. Tegmark, M. Zaldarriaga, and A. Hamilton, *Phys. Rev. D* **69**, 063516 (2004).
- [44] J.R. Weeks, arXiv:0412231.
- [45] L.R. Abramo, A. Bernui, I.S. Ferreira, T. Villela, and C.A. Wuensche, *Phys. Rev. D* **74**, 063506 (2006).
- [46] L.-Y. Chiang, P.D. Naselsky, O.V. Verkhodanov, and M.J. Way, *Astrophys. J.* **590**, L65 (2003).
- [47] P. Vielva, E. Martínez-González, R.B. Barreiro, J.L. Sanz, and L. Cayón, *Astrophys. J.* **609**, 22 (2004).
- [48] C.J. Copi, D. Huterer, and G.D. Starkman, *Phys. Rev. D* **70**, 043515 (2004).
- [49] M. Cruz, E. Martínez-González, P. Vielva, and L. Cayón, *Mon. Not. R. Astron. Soc.* **356**, 29 (2005).
- [50] M. Cruz, L. Cayón, E. Martínez-González, P. Vielva, and J. Jin, *Astrophys. J.* **655**, 11 (2007).
- [51] J.D. McEwen, M.P. Hobson, A.N. Lasenby, and D.J. Mortlock, *Mon. Not. R. Astron. Soc.* **371**, L50 (2006).
- [52] A. Bernui, C. Tsallis, and T. Villela, *Europhys. Lett.*, **78**, 19001 (2007).
- [53] E. Martínez-González, arXiv:0805.4157.
- [54] J.D. McEwen, M.P. Hobson, A.N. Lasenby, and D.J. Mortlock, *Mon. Not. R. Astron. Soc.* **388**, 659 (2008).
- [55] R. Aurich, S. Lustig, and F. Steiner, *Class. Quantum Grav.* **22**, 3443 (2005).
- [56] K. Land and J. Magueijo, *Mon. Not. R. Astron. Soc.* **367**, 1714 (2006).
- [57] T.R. Jaffe, A.J. Banday, H.K. Eriksen, K.M. Górski, and F. K. Hansen, *Astron. & Astrophys.* **460**, 393 (2006).
- [58] W.S. Hipólito-Ricaldi and G.I. Gomero, *Phys. Rev. D* **72**, 103008 (2005).
- [59] J.G. Cresswell, A.R. Liddle, P. Mukherjee, and A. Riazuelo, *Phys. Rev. D* **73**, 041302(R) (2006).
- [60] T. Ghosh, A. Hajian, and T. Souradeep, *Phys. Rev. D* **75**, 083007 (2007).
- [61] C. Gordon, W. Hu, D. Huterer, and T. Crawford, *Phys. Rev. D* **72**, 103002 (2005).
- [62] A.E. Gümrükçüoğlu, C.R. Contaldi, and M. Peloso, *J. Cosmol. Astropart. Phys.* **11**, 005 (2007).
- [63] A.R. Pullen and M. Kamionkowski, *Phys. Rev. D* **76**, 103529 (2007).
- [64] L. Ackerman, S.M. Carroll, and M.B. Wise, *Phys. Rev. D* **75**, 083502 (2007).
- [65] J.F. Donoghue, K. Dutta, and A. Ross, arXiv:0703455.
- [66] C. Dvorkin, H.V. Peiris, and W. Hu, *Phys. Rev. D* **77**, 063008 (2008).
- [67] M. Demiański and A.G. Doroshkevich, *Phys. Rev. D* **75**, 123517 (2007).
- [68] T. Kahniashvili, Y. Maravin, and A. Kosowsky, arXiv:0806.1876.
- [69] T. Kahniashvili, G. Lavrelashvili, and B. Ratra, arXiv:0807.4239.
- [70] T.S. Pereira, C. Pitrou, J.-P. Uzan, *JCAP* **09**, 006 (2007).
- [71] L. Campanelli, P. Cea, and L. Tedesco, *Phys. Rev. D* **76**, 063007 (2007).
- [72] J.A. Morales and D. Sáez, *Astrophys. J.* **678**, 583 (2008).
- [73] A. Bernui and W.S. Hipólito-Ricaldi, arXiv:0807.1076.
- [74] A. Rakić and D.J. Schwarz, *Phys. Rev. D* **75**, 103002 (2007).
- [75] H.K. Eriksen, A.J. Banday, K.M. Górski, and P.B. Lilje, *Astrophys. J.* **612**, 633 (2004).
- [76] T. Wibig and A.W. Wolfendale, *Mon. Not. R. Astron. Soc.* **360**, 236 (2005).
- [77] A. de Oliveira-Costa and M. Tegmark, *Phys. Rev. D* **74**, 023005 (2006).
- [78] M. Cruz, M. Tucci, E. Martínez-González, and P. Vielva, *Mon. Not. R. Astron. Soc.* **369**, 57 (2006).
- [79] L.R. Abramo, L. Sodr e Jr., and C.A. Wuensche, *Phys. Rev. D* **74**, 083515 (2006).
- [80] L.-Y. Chiang, P. Coles, P.D. Naselsky, and P. Olesen, *JCAP* **1**, 21 (2007).
- [81] M. L opez-Corredoira, *J. Astrophys. Astron.* **28**, 101 (2007).
- [82] R.C. Helling, P. Schupp, and T. Tesileanu, *Phys. Rev. D* **74**, 063004 (2006).
- [83] E.F. Bunn, *Phys. Rev. D* **75**, 083517 (2007).
- [84] P.D. Naselsky, O.V. Verkhodanov, and M.T.B. Nielsen, arXiv:0707.1484.
- [85] D.J. Schwarz, G.D. Starkman, D. Huterer, and C.J. Copi, *Phys. Rev. Lett.* **93**, 221301 (2004).
- [86] P. Bielewicz *et al.*, *Astrophys. J.* **635**, 750 (2005).
- [87] K.M. Górski *et al.*, *Astrophys. J.* **622**, 759 (2005).
- [88] T. Padmanabhan, *Structure formation in the universe*, (Cambridge Univ. Press, Cambridge, 1993).
- [89] J. Kim, P. Naselsky, and P.R. Christensen, *Phys. Rev. D* **77**, 103002 (2008).